# Surface to sewer flow exchange through circular inlets during urban flood conditions

Matteo Rubinato, Seungsoo Lee, Ricardo Martins and James D. Shucksmith

## ABSTRACT

Accurately quantifying the capacity of sewer inlets (such as manhole lids and gullies) to transfer water is important for many hydraulic flood modelling tools. The large range of inlet types and grate designs used in practice makes the representation of flow through and around such inlets challenging. This study uses a physical scale model to quantify flow conditions through a circular inlet during shallow steady state surface flow conditions. Ten different inlet grate designs have been tested over a range of surface flow depths. The resulting datasets have been used (i) to quantify weir and orifice discharge coefficients for commonly used flood modelling surface–sewer linking equations and (ii) to validate a 2D finite difference model in terms of simulated water depths around the inlet. Calibrated weir and orifice coefficients were observed to be in the range 0.115–0.372 and 0.349–2.038, respectively, and a relationship with grate geometrical parameters was observed. The results show an agreement between experimentally observed and numerically modelled flow depths but with larger discrepancies at higher flow exchange rates. Despite some discrepancies, the results provide improved confidence regarding the reliability of the numerical method to model surface to sewer flow under steady state hydraulic conditions.

**Key words** | discharge coefficients, experimental modelling, numerical modelling, surface to sewer flow exchange, urban flooding

**Matteo Rubinato**
**Ricardo Martins**
**James D. Shucksmith**
Civil and Structural Engineering Department,
The University of Sheffield,
Sir Frederick Mappin Building, Mappin Street,
S1 3JD Sheffield,
UK

**Seungsoo Lee** (corresponding author)
APEC Climate Center,
12 Centum 7-ro, Haeundae-gu, Busan 612-020,
Republic of Korea, 48058
E-mail: *seungsoo_lee@apcc21.org*

**Ricardo Martins**
MARE – Marine and Environmental Sciences Centre, Department of Civil Engineering, FCT,
University of Coimbra,
Coimbra,
Portugal
and
IMAR – Institute of Marine Research, FCT,
University of Coimbra,
Coimbra,
Portugal

## INTRODUCTION

Current climatic trends mean that the frequency and magnitude of urban flooding events is forecast to increase in the future (Hammond *et al.* 2015) leading to increased damage in terms of loss of business, livelihoods plus increased inconvenience for citizens (Ten Veldhuis & Clemens 2010). These potential impacts underline the importance of accurate modelling tools to determine flow paths within and between overland surfaces and sewer/drainage systems. Existing urban flood models commonly utilise the 1D Saint-Venant and 2D Shallow Water Equations (SWE) to calculate flows within sewer pipes and on the surface (overland flow) (Martins *et al.* 2017b). However, modelers are also faced with the concern of how to correctly reproduce the hydraulic behaviour around and within complex and variable hydraulic structures such as manholes and gullies which are used to connect the surface system to the sewer system. Unless the inlet is blocked or the sewer is surcharged, these structures allow water to be drained from the surface. An inaccurate representation of inlet capacity can lead to incorrect prediction of flow volumes, velocities and depths on the surface (Xia *et al.* 2017), as well as in the sewer pipes. Due to their geometrical complexity such linking structures are conventionally represented using weir and orifice equations within urban flood models (Djordjević *et al.* 2005;

doi: 10.2166/hydro.2018.127

Chen et al. 2007; Leandro et al. 2009; Martins et al. 2017a). However, due to a paucity of datasets, the robust calibration and validation of such linking methodologies is lacking. In particular, the determination of appropriate discharge coefficients for such linking equations over a range of hydraulic conditions and inlet types is required.

Experimental studies investigating surface–sewer flow interaction via gullies and manholes are scarce (Martins et al. 2014). Larson (1947) identified inlet width and the efficiency of the inlet opening as characteristics of primary importance to determine inlet capacity; Li et al. (1951, 1954) experimentally investigated the effectiveness of some grate inlets in transferring flow from surface to sewer by treating the flow bypassing the grate as separate portions, and Guo (2000a, 2000b) and Almedeij & Houghtalen (2003) proposed different modifications to grate inlet design. Gómez & Russo (2009) investigated the hydraulic efficiency of transverse grates within gully systems proposing new mathematical expressions to define the hydraulic efficiency. Gómez & Russo (2011a) studied the hydraulic behaviour of inlet grates in urban catchments during storm events and Gómez et al. (2011b) presented an empirical relationship to obtain the hydraulic efficiency as a function of inlet and street flow characteristics. In further work, Gómez et al. (2013) investigated the hydraulic efficiency reduction as a result of partially clogged grate inlets. More recently, Rubinato et al. (2017a) experimentally validated the ability of weir/orifice linking equations to represent steady flow exchange through a scaled open manhole. However, the performance was dependent on the calibration of the discharge coefficients as well as a robust characterisation of the flow within the sewer and flow depth on the surface such that the hydraulic head difference between surface and sewer flows could be accurately determined. An accurate representation of flow exchange is therefore also dependent on correctly modelling of flow conditions (hydraulic head) in the vicinity of the inlet structure.

Literature published to date lacks repeatable tests of different grate inlets under controlled conditions and an integration of results into modelling tools. Numerical studies of flows around gullies and manholes are limited due to a lack of experimental data as well as long computational times when simulating complex 3D flows (Leandro et al. 2014). However, some studies have been conducted: Lopes et al. (2015) analysed experimental results from a surcharging jet arising from the reverse flow out of a manhole after the sewer system became pressurised; Djordjević et al. (2013) focused on surface recirculation zones formed downstream of gullies; both studies have used experimental data to model flow patterns inside gullies and manholes using computational fluid dynamics (CFD); Rubinato et al. (2016) studied flow depths around an open circular manhole under drainage conditions and validated a 2D finite difference model. Martins et al. (2017a) validated two finite volume (FV) flood models in the case where horizontal floodplain flow is affected by sewer surcharge flow via a manhole demonstrating that the shock capturing FV-based flood models are applicable tools to model localised sewer-to-floodplain flow interaction. However, no studies to date have looked specifically at the influence of different grate cover designs/geometries on flow exchange capacity, flow conditions around the inlet and the ability of 2D modelling tools to replicate depths around the inlet over a range of flows.

The objective of this work is to use a physical scale model to collect an extensive series of experimental datasets describing surface to sewer flow exchange through a circular inlet under steady state conditions through ten different inlet grate configurations. The datasets are used to (i) determine appropriate weir/orifice discharge coefficients applicable to describe exchange flows and (ii) validate the ability of a calibrated 2D numerical finite difference method (FDM) to describe observed surface flow depths in the vicinity of the inlet structure.

## METHODOLOGY

This section presents (i) the experimental facility used to collect the data, (ii) hydraulic conditions for the tests conducted, (iii) a detailed procedure of the methods used to estimate discharge coefficients of the linking equations and (iv) a description of the numerical flood model utilised.

### Experimental model

The experimental set-up utilised (Figure 1) was assembled at the water laboratory of the University of Sheffield (UK) (Rubinato 2015). It consists of a scaled model of an urban

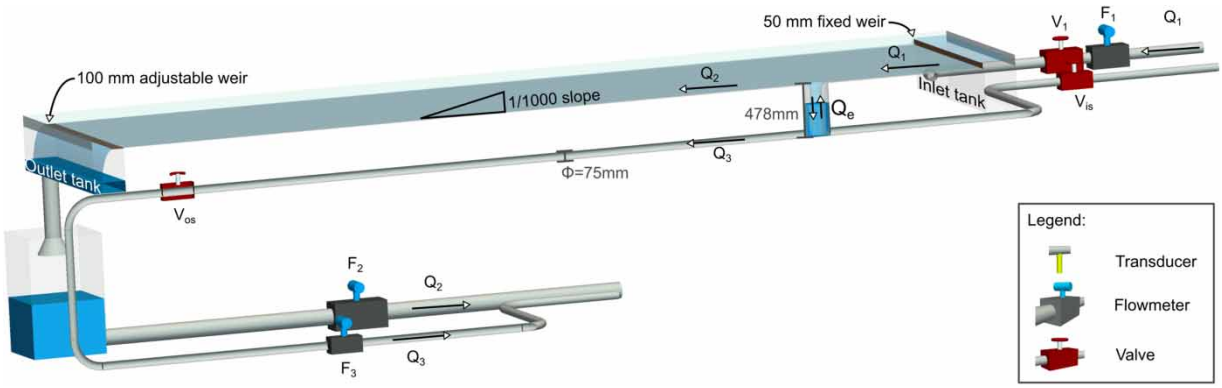


**Figure 1** | Scheme of the experimental facility (Rubinato *et al.* 2017b).

drainage system/floodplain linked via a manhole shaft. The floodplain surface (4 m, width, by 8.2 m, length) has a longitudinal slope of 1/1000. The urban drainage system is made from horizontal acrylic pipes directly beneath the surface (inner diameter = 0.075 m). One circular acrylic shaft (representing a manhole) with 0.240 m inner diameter and 0.478 m height connects the surface to the pipes. The facility is equipped with a SCADA system (Supervision, Control and Data Acquisition) through Labview™ software that permits the setup and monitoring of flow rates within the surface and sewer systems independently. A pumping system in a closed circuit supplies water within the facility. The inlet pipes ($V_1$, $V_{is}$) are fitted with electronic control valves operated via Labview™ software. The surface downstream outlet is a free outfall which contains an adjustable height weir.

Calibrated electro-magnetic (MAG) flow meters ($F_1$, inlet floodplain; $F_2$, outlet floodplain; $F_3$ outlet sewer) were installed in the upstream and downstream pipes in order to measure the surface system inflow ($Q_1$) and surface and sewer outflows ($Q_2$, $Q_3$) and calculate the steady state drainage rate through the surface to sewer inlet ($Q_e$). Each flow meter was independently verified against a laboratory measurement tank. For the tests reported here, the sewer inflow was not used (sewer inflow = 0) and all flow therefore entered the facility via the surface inlet weir ($Q_1$). Drainage flow passed via the drainage inlet to the sewer outlet ($Q_e = Q_3$), with the remaining flow passing over the facility to downstream outlet weir ($Q_2$). Flow depth on the floodplain was measured by a series of pressure sensors (of type GEMS series 5000) fitted at various locations around the inlet (Figure 2) (with an accuracy of ±0.109 mm for the range of water depth 0–100 mm). Ten different grate types were constructed from acrylic using a laser cutter and installed within the drainage structure and tested under steady state conditions in order to obtain flow depth vs drainage discharge ($Q_e$) relationships for each grate type. The grate opening types were selected based on common types used in different countries, and are presented in Figure 3.

For each grate opening type the total area of empty space ($A_e$) and total effective edge perimeter length ($P_v$) were obtained from the AutoCAD drawings prior to fabrication (Table 1). Autocad drawings are included as supplementary data (available with the online version of this paper).

## Hydraulic conditions

For each grate inlet displayed in Figure 3, eight tests have been completed over a range of surface inflows ($Q_1$) between 4 and 10 l/s set using the upstream valve ($V_1$). This is equivalent to a unit width discharge ($q_1 = Q_1/B$) between 1 and 2.5 l/s. To ensure reliable depth and flow rate quantification for each test, flows were left to stabilise for 5 minutes before flow rates and depths were recorded. Each reported depth/flow measurement is a temporal average of 3 minutes of recorded data after flow stabilisation, such that full convergence of measured parameters is achieved.

In all cases, a flat weir was used as the downstream floodplain boundary, and free surface flow was maintained in the pipe system.

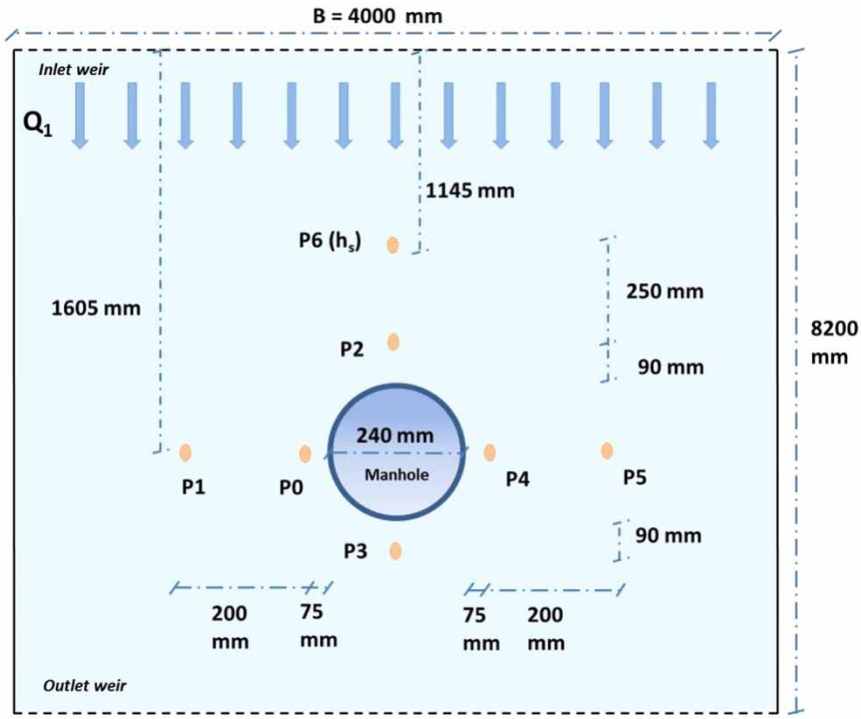


**Figure 2** | Location of the pressure transducer measurement points around the surface to sewer drainage inlet (not to scale).

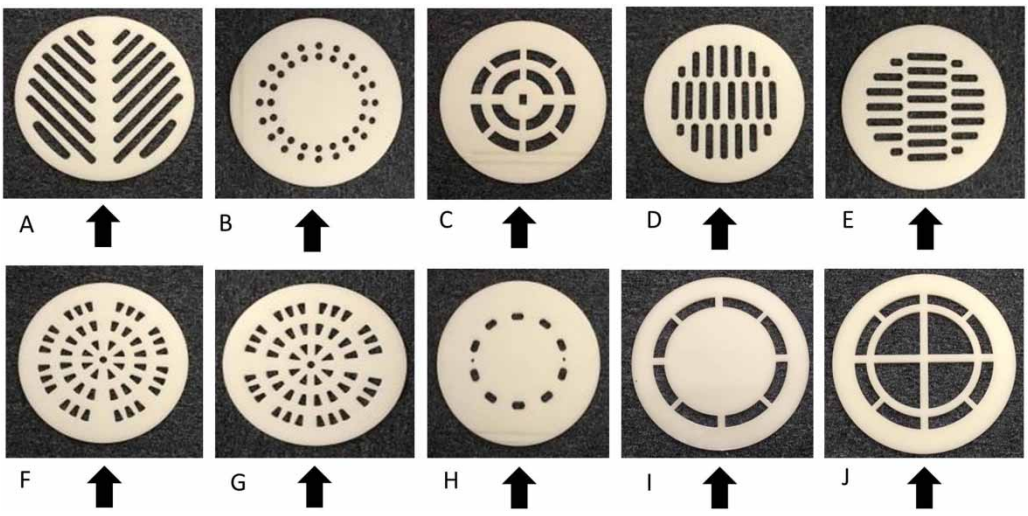


**Figure 3** | Grates applied on the top of the inlet (black arrows show the primary direction of the facility inflow $Q_1$ and hence the orientation of each inlet grate).

The upstream flow depth ($h_s$) is reported as the depth recorded at transducer *P6* (Figure 2). Surface flow Froude number (*Fr*) is calculated based on this flow depth and the calculated cross-sectional averaged velocity ($U$) at this position ($U = Q_1/B.h_s$). The hydraulic conditions for each test are detailed in Table 2. Full (non-averaged) datasets from flow meters $Q_1$, $Q_3$ and transducers ($P_0$, $P_1$, $P_2$, $P_3$, $P_4$, $P_5$, $P_6$) are presented as supplementary data (Table S1) to this paper.

**Table 1** | Technical details of the grids utilised

| Grate | Area filled $A_f$ (m$^2$) | Area empty spaces $A_e$ (m$^2$) | Void ratio $V$ (%) | Effective perimeter $P_v$ (m) |
|---|---|---|---|---|
| A | 0.0307 | 0.0145 | 32.1 | 3.0364 |
| B | 0.0421 | 0.0031 | 6.9 | 1.2520 |
| C | 0.0373 | 0.0079 | 17.48 | 1.3880 |
| D | 0.0353 | 0.0099 | 21.9 | 2.3794 |
| E | 0.0353 | 0.0099 | 21.9 | 2.3794 |
| F | 0.0391 | 0.0061 | 13.5 | 2.2586 |
| G | 0.0391 | 0.0061 | 13.5 | 2.2586 |
| H | 0.0435 | 0.0017 | 3.76 | 0.5128 |
| I | 0.0385 | 0.0067 | 14.11 | 1.2428 |
| J | 0.0277 | 0.0175 | 38.03 | 1.8816 |

## Discharge coefficients

Within flood modelling applications the weir (1) and orifice (2) equations are commonly defined as the following (Rubinato *et al.* 2017a):

$$Q_e = \frac{2}{3} C_w \pi D_m \sqrt{2g} (H)^{3/2} \tag{1}$$

where $D_m$ is the diameter of the (circular) inlet (m), $H$ is the driving hydraulic head above the interface point accounting for both sewer and surface flows (m). $C_w$ is the weir discharge coefficient.

$$Q_e = C_o A_m \sqrt{2gH} \tag{2}$$

where $A_m$ is the open area of the inlet and $C_o$ is the orifice coefficient. In cases where the sewer is not surcharged, the hydraulic head ($H$) is assumed to be equal to the surface flow depth.

To calibrate discharge coefficients for each grate type, Equations (2) and (3) were modified to account for the total length of the weir within each grate design (taken as equal to $P_v$) and total open area (taken as equal to $A_e$). The flow depth is taken as the measured upstream value ($h_s$).

$$Q_e = \frac{2}{3} C_w P_V \sqrt{2g} (h_s)^{3/2} \tag{3}$$

$$Q_e = C_o A_e \sqrt{2g} (h_s)^{1/2} \tag{4}$$

## Numerical model

The depth-averaged 2D SWEs are commonly used for modelling flows in urban environments and in rivers and floodplains (Wang *et al.* 2011). Integrating an inflow and outflow in/from the sewerage system can be realised by adding suitable source terms (Lee *et al.* 2013). The governing equations used for floodplain modelling with surface to sewer inflows are as follows:

$$\frac{\partial h}{\partial t} + \frac{\partial (uh)}{\partial x} + \frac{\partial (vh)}{\partial y} = -q_e \tag{5}$$

$$\frac{\partial (uh)}{\partial t} + \frac{\partial (u^2 h)}{\partial x} + \frac{\partial (uvh)}{\partial y} = -gh \frac{\partial E}{\partial x} - gn^2 \frac{u\sqrt{u^2+v^2}}{h^{1/3}} \tag{6}$$

$$\frac{\partial (vh)}{\partial t} + \frac{\partial (uvh)}{\partial x} + \frac{\partial (v^2 h)}{\partial y} = -gh \frac{\partial E}{\partial y} - gn^2 \frac{v\sqrt{u^2+v^2}}{h^{1/3}} \tag{7}$$

In Equations (5)–(7), $(x, y)$ are the spatial Cartesian coordinates and $t$ is the time (SI units). $h$ (m) is the water depth $u$ and $v$ (m/s) are $x$- and $y$-direction velocities, respectively. $E$ is the water elevation (m), and $n$ is Manning's roughness coefficient (here taken as 0.009 m/s$^{1/3}$, from previous experimental work, e.g., Rubinato *et al.* (2017a)). $q_e$ (m/s) is the area discharge, in this study representing surface to sewer discharge via the inlet grate.

A leap-frog method is used in order to reduce simulation time, with variables laid on staggered mesh. Fluxes ($uh$ and $vh$) are located at the computational cell boundary and water depth ($h$) is located at the centre of the computational cell. More detailed information regarding the leap-frog and FDM methods can be found in Lee (2013).

### Model setup and boundary conditions

An adaptive mesh technique (Haleem *et al.* 2015) is used to reduce the calculation time (Figure 4). In the simulation, the downstream depth measurement point (*P7*) is used to define downstream boundary conditions, hence the initial number of quadrilaterals was chosen to be $72 \times 40$ (7.2 m $\times$ 4.0 m) to generate a baseline (coarse) mesh with a spatial resolution of around 0.1 m $\times$ 0.1 m. A mesh

**Table 2** | Hydraulic parameters measured ($Q_1$, $Q_e$ and $h_s$) and calculated ($Fr$) for the tests conducted

| Grate | $Q_1$ (l/s) | $Q_e$ (l/s) | $h_s$ (mm) | $Fr$ (/) | Grate | $Q_1$ (l/s) | $Q_e$ (l/s) | $h_s$ (mm) | $Fr$ (/) |
|---|---|---|---|---|---|---|---|---|---|
| A | 4.33 | 0.55 | 7.28 | 0.556 | B | 4.29 | 0.50 | 7.26 | 0.554 |
| | 5.00 | 0.67 | 7.89 | 0.569 | | 4.99 | 0.59 | 7.92 | 0.565 |
| | 5.66 | 0.76 | 8.50 | 0.576 | | 5.67 | 0.68 | 8.60 | 0.568 |
| | 6.32 | 0.86 | 9.09 | 0.582 | | 6.33 | 0.76 | 9.15 | 0.577 |
| | 6.93 | 0.93 | 9.49 | 0.599 | | 6.93 | 0.82 | 9.63 | 0.586 |
| | 7.51 | 0.94 | 10.05 | 0.595 | | 7.52 | 0.89 | 10.12 | 0.590 |
| | 8.22 | 1.05 | 10.60 | 0.601 | | 8.18 | 0.91 | 10.64 | 0.596 |
| | 9.29 | 1.19 | 11.36 | 0.612 | | 9.22 | 0.94 | 11.42 | 0.603 |
| C | 4.29 | 0.43 | 7.53 | 0.524 | D | 4.23 | 0.43 | 7.72 | 0.498 |
| | 4.97 | 0.54 | 8.16 | 0.539 | | 4.96 | 0.59 | 8.40 | 0.514 |
| | 5.66 | 0.63 | 8.91 | 0.538 | | 5.69 | 0.70 | 9.24 | 0.512 |
| | 6.32 | 0.72 | 9.53 | 0.542 | | 6.30 | 0.72 | 10.11 | 0.495 |
| | 6.95 | 0.74 | 10.10 | 0.546 | | 6.96 | 0.80 | 10.72 | 0.501 |
| | 7.54 | 0.80 | 10.60 | 0.552 | | 7.49 | 0.82 | 11.18 | 0.506 |
| | 8.21 | 0.88 | 11.14 | 0.558 | | 8.19 | 0.96 | 11.70 | 0.516 |
| | 9.28 | 0.97 | 11.91 | 0.570 | | 9.24 | 1.09 | 12.49 | 0.529 |
| E | 4.27 | 0.44 | 7.36 | 0.540 | F | 4.28 | 0.44 | 7.40 | 0.537 |
| | 5.00 | 0.53 | 8.02 | 0.555 | | 4.95 | 0.48 | 8.07 | 0.545 |
| | 5.68 | 0.63 | 8.62 | 0.566 | | 5.66 | 0.61 | 8.75 | 0.552 |
| | 6.31 | 0.69 | 9.19 | 0.572 | | 6.37 | 0.70 | 9.40 | 0.558 |
| | 6.96 | 0.77 | 9.70 | 0.582 | | 6.96 | 0.85 | 9.74 | 0.577 |
| | 7.51 | 0.81 | 10.01 | 0.582 | | 7.52 | 0.90 | 10.20 | 0.582 |
| | 8.19 | 0.90 | 10.59 | 0.600 | | 8.17 | 0.95 | 10.63 | 0.595 |
| | 9.24 | 0.99 | 11.42 | 0.605 | | 9.25 | 1.10 | 11.49 | 0.599 |
| G | 4.22 | 0.48 | 7.60 | 0.508 | H | 4.26 | 0.39 | 7.25 | 0.551 |
| | 4.93 | 0.61 | 8.27 | 0.523 | | 4.97 | 0.44 | 7.96 | 0.558 |
| | 5.63 | 0.72 | 9.01 | 0.525 | | 5.66 | 0.48 | 8.68 | 0.559 |
| | 6.26 | 0.80 | 9.61 | 0.530 | | 6.29 | 0.52 | 9.35 | 0.555 |
| | 6.87 | 0.84 | 10.05 | 0.544 | | 6.92 | 0.58 | 9.82 | 0.567 |
| | 7.52 | 0.94 | 10.50 | 0.558 | | 7.51 | 0.66 | 10.30 | 0.574 |
| | 8.21 | 1.03 | 11.00 | 0.568 | | 8.19 | 0.68 | 10.77 | 0.584 |
| | 9.22 | 1.13 | 11.76 | 0.578 | | 9.22 | 0.70 | 11.57 | 0.592 |
| I | 4.26 | 0.43 | 7.28 | 0.547 | J | 4.26 | 0.46 | 7.44 | 0.530 |
| | 4.97 | 0.57 | 7.85 | 0.571 | | 4.94 | 0.52 | 8.13 | 0.538 |
| | 5.64 | 0.63 | 8.53 | 0.571 | | 5.66 | 0.64 | 8.78 | 0.549 |
| | 6.27 | 0.71 | 9.13 | 0.573 | | 6.27 | 0.72 | 9.39 | 0.550 |
| | 6.92 | 0.78 | 9.65 | 0.583 | | 6.91 | 0.77 | 9.87 | 0.562 |
| | 7.51 | 0.88 | 10.08 | 0.593 | | 7.52 | 0.90 | 10.35 | 0.570 |
| | 8.16 | 0.93 | 10.58 | 0.599 | | 8.18 | 0.95 | 10.84 | 0.579 |
| | 9.22 | 1.03 | 11.39 | 0.605 | | 9.21 | 0.98 | 11.66 | 0.584 |

convergence analysis was carried out, which suggested the need for a four times finer mesh for the model to be able to appropriately resolve the hydrodynamics of the grate inlet. As shown in Figure 4, up to four levels of refinement are implemented around the local zone of sewer-to-floodplain interaction (resolution around $6.25\,\text{mm} \times 6.25\,\text{mm}$) and these are assumed appropriate to replicate the geometry of each grate type. The open cells within each grate area are identified as cells where the $q_e$ term in Equation (5) is non-zero. The total flow exchange from surface to sewer is calculated by applying Equation (3) using the experimentally obtained weir coefficients and simulated upstream water depth at *P6* ($h_s$). $q_e$ for each open cell is then calculated based on the total calculated flow exchange and the total open area of each grate type. All the simulations were run until convergence to a steady state is attained. A mesh

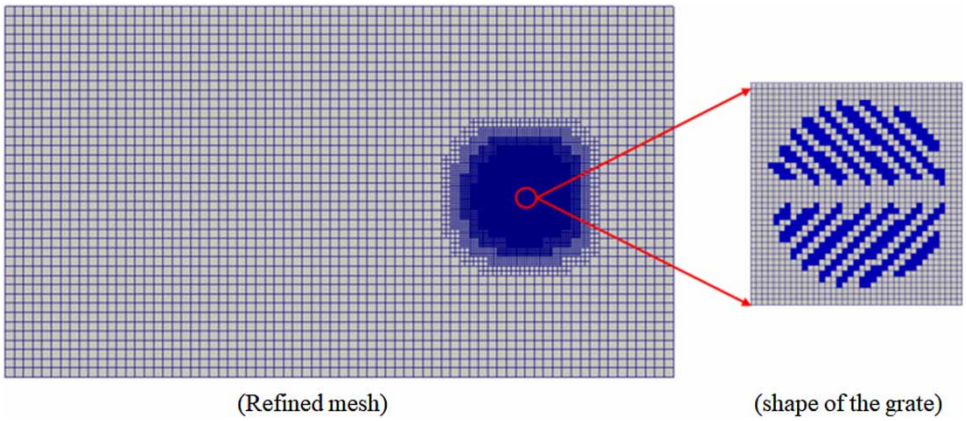


**Figure 4** | Mesh characterisation example for grate type A.

convergence analysis suggested the use of a convergence (depth) threshold-error no bigger than $10^{-4}$ and no less than $10^{-6}$. The initial discharge condition is taken to be the unit width surface inflow $q_1$ and a measured velocity profile is used to set water depth at the eastern (upstream) boundary. This velocity curve was obtained prior to the experiments by measuring ten flows ($Q_1$) between 2 l/s and 11 l/s and recording the average velocity in the area included between 0.5 and 3.5 m of the total width, with sampling points each 0.5 m. At the southern and northern boundaries (lateral), a wall boundary condition is employed (reflective). At the western (downstream) boundary, measured water depth at *P7* is used.

## RESULTS AND DISCUSSION

This section presents discharge coefficients estimated for each grate configuration and the comparison of the 2D finite difference model predictions against observed flow depths recorded around the inlet at seven different pressure sensor locations (*P0–P6*) displayed in Figure 2.

### Experimental results and calibrated discharge coefficients

Figure 5 shows the relationship between the upstream water depth ($h_s$) and the correspondent flow exchange ($Q_e$) through each grate type over the range of flow conditions tested. The results confirm that the geometry of each grate

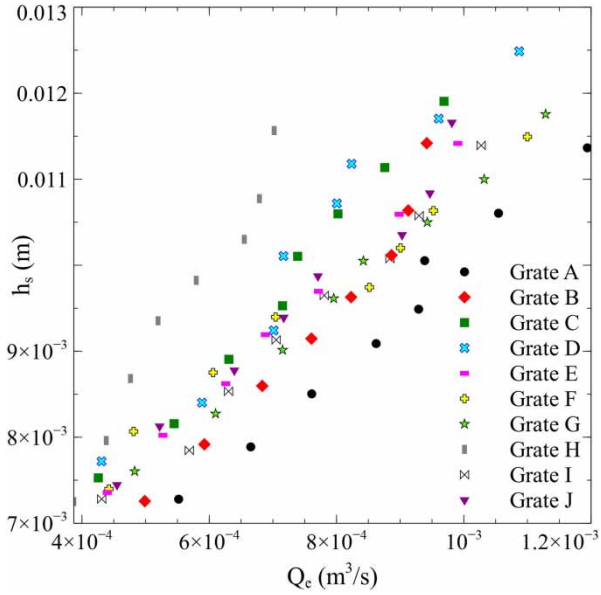


**Figure 5** | The observed relationship between upstream water depth vs surface to sewer flow exchange for each grate type.

strongly influences the flow entering the surface-sewer inlet. When comparing results for similar hydraulic conditions, *grate H* ($A_e = 0.0017$ m$^2$; $P_v = 0.5128$ m) is the grate that results in the lowest exchange flows while *grate A* allows the highest exchange flows ($A_e = 0.0145$ m$^2$; $P_v = 3.0364$ m). It can be noted that while *grate A* has the highest perimeter values, its void area is lower than *grate J*. In general, the results confirm that the exchange flow capacity of each grate design is more strongly correlated to the effective perimeter than the void area; however, individual different grate designs can affect the flow patterns around the void

spaces and hence drainage efficiency. To provide a better understanding of this a further investigation including consideration of the local flow velocity is required.

Calibration of Equations (3) and (4) is achieved by fitting a linear trend between the terms of the relevant equation and the surface to sewer exchange flow ($Q_e$) for each grate type (shown in Figure 6). The average goodness of fit of the linkage equations over all grate types (weir equation average $R^2 = 0.977$, orifice equation $R^2 = 0.980$) shows that both weir and orifice equations are shown to be applicable for representation of surface to sewer flow exchange in steady flow (confirming previous work, Rubinato *et al.* (2017a)) and that over the range of hydraulic conditions tested here, the weir and orifice coefficients can be taken as constant. Calibrating the weir Equation (3) against the experimental results provides a discharge coefficient $C_w$ in the range 0.115–0.372 based on the variety of grates applied (Table 1). Calibration of the orifice Equation (4) against the experimental results provides a discharge coefficient $C_o$ in the range 0.349–2.038. Values for each grate type are provided in Table 3, along with correspondent goodness of fit values ($R^2$).

Discharge coefficients observed in this study are in the same range to those found by Martins *et al.* (2014) for a $0.6 \times 0.3 \times 0.3$ m gully under drainage conditions ($0.16 < C_w < 1.00$, $1.36 < C_o < 2.68$) but differs to those obtained by Bazin *et al.* (2014) for small ($0.05 \times 0.05$ m) fully open street inlets ($0.58 < C_o < 0.67$). This is likely due to the variation in scales between the experimental facilities used.

It is noticeable that the orifice equation results in a larger variation in the range of calibrated coefficients than the weir equation. Calibrated discharge coefficients show an inverse trend with the geometrical parameters ($P_v$ or $A_e$) associated with the different grate types, suggesting a higher energy loss associated with surface to sewer flow transfer as opening size decreases (Figure 7). Figure 7 shows that coefficients approach an approximately constant value ($C_w \approx 0.115$, $C_o \approx 0.35$ in this case) as opening size and size and perimeter length increases. The consideration of individual grate types shows that the application of the weir equation tends to provide higher $R^2$ values for grate types when the perimeter length value ($P_v$) is relatively large (e.g., grate types *D* and *G*), while the orifice equation tends to provides higher $R^2$ values for grate types when the perimeter length value is smaller (e.g., grate types *B*

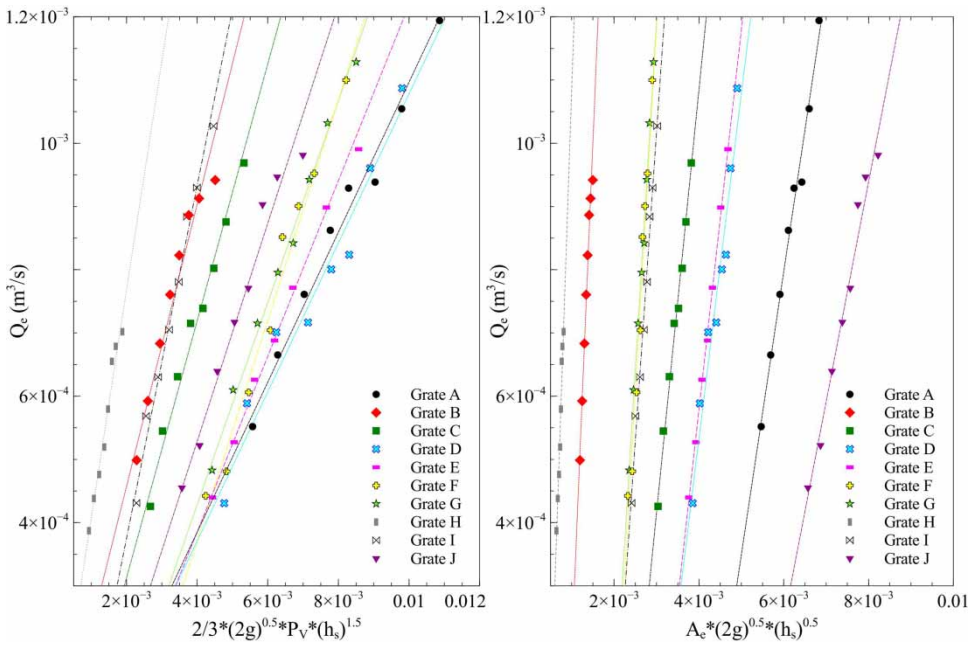


**Figure 6** | The relationship between the weir Equation (3) for each flow condition tested vs the correspondent flow exchange (left); the relationship between the orifice Equation (4) vs the correspondent flow exchange (right).

**Table 3** | Values of experimentally calibrated weir and orifice coefficients ($C_w$ and $C_o$) and correspondent goodness of fit $R^2$ values

| Grate | $C_w$ | $R^2$ | $C_o$ | $R^2$ |
|---|---|---|---|---|
| A | 0.115 | 0.984 | 0.448 | 0.987 |
| B | 0.208 | 0.951 | 1.546 | 0.974 |
| C | 0.194 | 0.985 | 0.657 | 0.991 |
| D | 0.115 | 0.957 | 0.552 | 0.950 |
| E | 0.135 | 0.995 | 0.606 | 0.998 |
| F | 0.204 | 0.981 | 1.115 | 0.994 |
| G | 0.157 | 0.995 | 1.222 | 0.976 |
| H | 0.372 | 0.966 | 2.038 | 0.967 |
| I | 0.264 | 0.989 | 0.969 | 0.989 |
| J | 0.168 | 0.969 | 0.349 | 0.978 |

and $C$). This may be due to the increased likelihood of grates with small effective perimeters to become 'drowned'. However, the effect is relatively subtle and in some cases the difference in $R^2$ values is negligible even between designs with large or small effective perimeter values (e.g., grate types $A$ and $H$).

## Numerical results

Figure 8 displays the difference between the experimental depths, as measured by the transducers (Figure 2), with the depths calculated by the numerical model at each measurement location ($h_{exp}$–$h_{sim}$). In most locations the numerical results overestimate the experimentally observed water depths. At locations *P0* and *P4* (i.e., 75 mm left and right of the inlet), this condition is reversed and the model tends to underestimate observed water depths. Despite this, overall, the numerical model provides a good representation of the experimental observations within the range of 0–5 mm of the experimental values when considering the full range of inlet flow conditions ($Q_1$). Modelling errors may be due to the uncertainties related to: (i) the replication of grates and the correspondent discretisation of the meshing system adopted; (ii) discrepancies in the floodplain bed elevation applied within the model; (iii) minor effects due to any skewed inflow from the inlet tank in the experimental model; (iv) use of the upstream water depth to calculate total flow exchange instead of actual hydraulic head at each exchange cell as well as any discharge coefficient calibration errors; (v) the depth averaged nature of the model or other simplifications. Errors are generally seen to be smaller for the range of $Q_1 = [4.2; 7.46]$ l/s. By analysing each measurement location separately, *P2* and *P3* (i.e., just upstream and downstream of the inlet) show the highest discrepancies (up to 5 mm). This may be related to complex flow patterns forming upstream and downstream of the inlet (such as water accumulation and separation and merging of stream flows) that the model may find difficult to fully replicate.

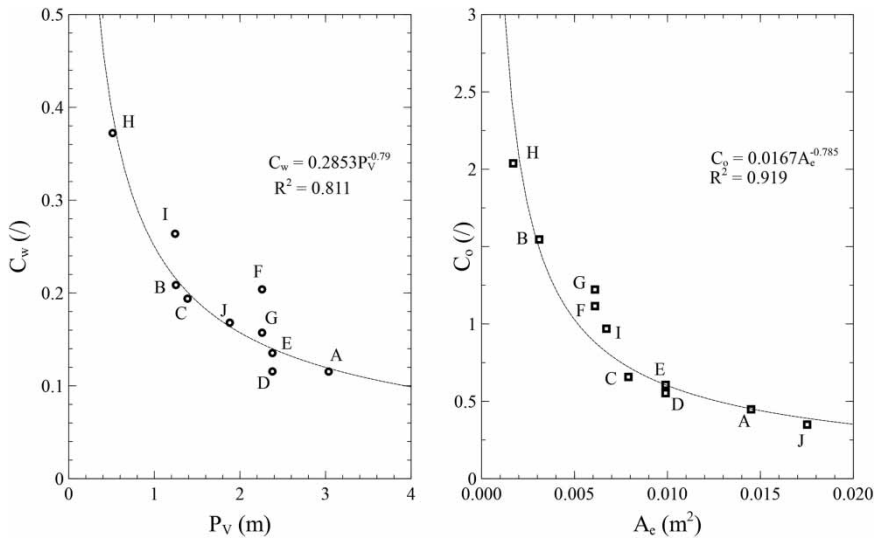


**Figure 7** | Relationships between experimentally calibrated weir ($C_w$) and orifice ($C_o$) coefficients and geometrical parameters for each inlet grate.

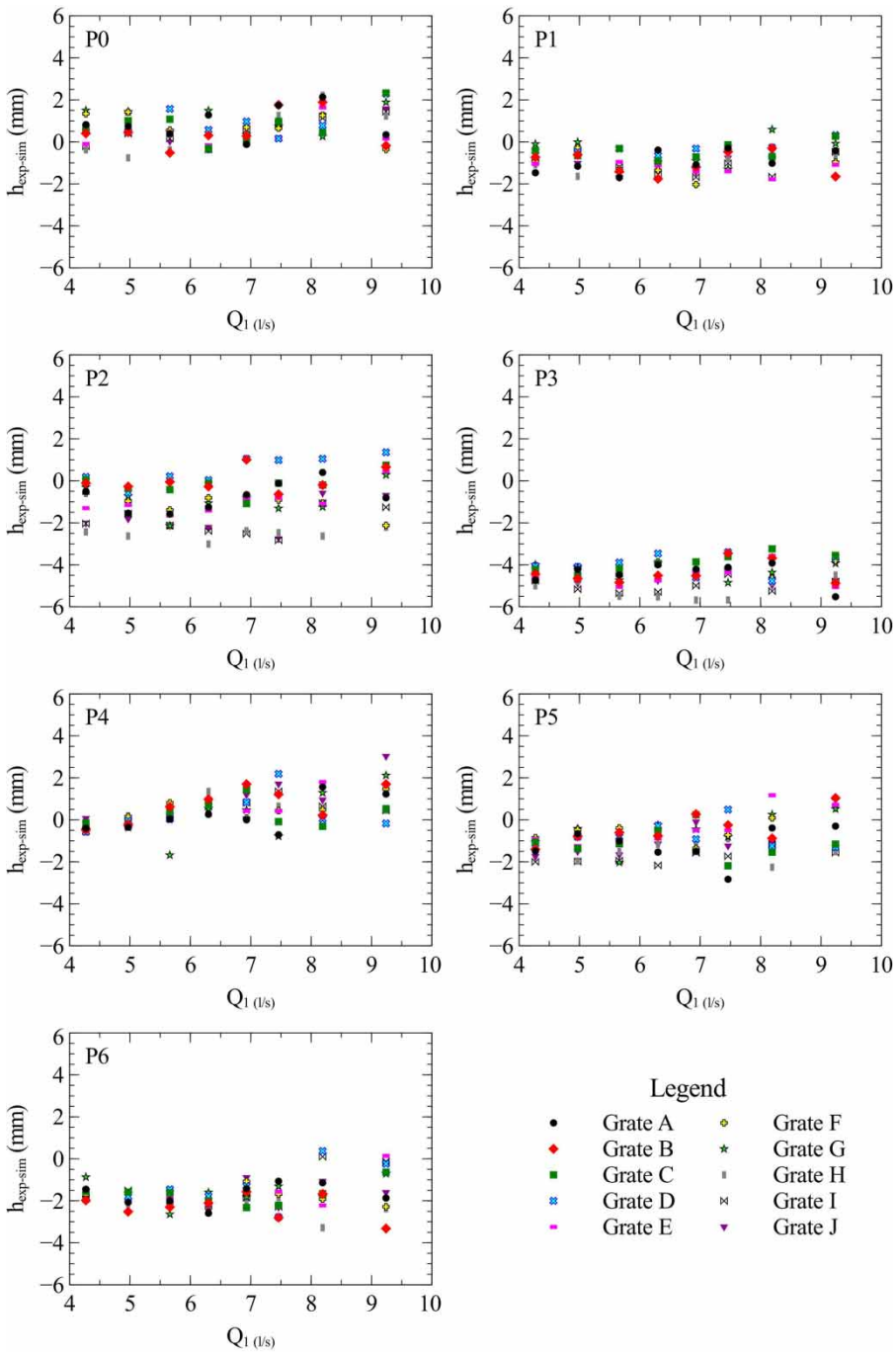


**Figure 8** | Comparison between the experimental observations and numerical hydraulic heads at each measurement location.

Discrepancies (0–3 mm) are also noted within the pressure measurement *P6* located 460 mm upstream of the centreline of the inlet. For measurement locations less influenced by the flow entering the inlet, such as *P1* and *P5*, errors are within the range 0–2 mm.

In terms of flow exchange rate, the numerical simulations tend to overestimate the average exchange discharge (on average by 0.25 l/s). Flow exchange calculations within modelling tools are sensitive to calculations of relative head within pipe and surface systems (Rubinato

et al. 2017a). In this case, flow exchange is calculated using the calibrated weir equation based on the numerical simulation of flow depth upstream of the inlet. Resulting discrepancies in the simulation of hydraulic water depths around the inlet can therefore be seen to propagate to the calculation of flow exchange rate.

## SUMMARY AND CONCLUSIONS

This work has explored the experimental and numerical modelling of surface to sewer flow exchange. A physical model, linking a slightly inclined urban floodplain to a sewer system, was used to carry out measurements under steady state flow conditions with the application of ten different circular grates on the top of a surface/sewer linking structure. Eighty steady state experiments were conducted, during which water levels at seven locations surrounding the inlet structure were measured. The results have confirmed the validity of both the weir and orifice linking equations to describe the total surface to sewer exchange flows through different inlet grates. Calibrated discharge coefficients have been provided for each grate type tested which were taken as constant over the range of hydraulic conditions tested. Overall, the calibrated orifice discharge coefficient showed a larger variation between the grate types. Whilst some evidence was provided to suggest that the weir equation outperforms the orifice equation when the effective perimeter of the grate is relatively high, and vice versa, no significant difference in performance was observed over the range of flow rates tested. Overall trends suggested that discharge coefficients (i.e. energy losses) decrease as the grate geometrical parameters (void area and effective perimeter) increase and may converge to an approximately constant value. In addition, a finite difference numerical model was tailored to reproduce flow conditions around the inlet structure. Experimentally calibrated exchange equations were used to define the inflow through each modelled grate type. The numerical results have been compared with the experiments in terms of depth around the inlet at seven sampling points and detailed comparisons show a regular agreement between the numerical and experimental water levels (maximum discrepancy 5 mm). It can therefore be concluded that the proposed 2D numerical approach is able to model floodplain-to-sewer interaction and flow conditions in the vicinity of the linking structure reliably, despite the uncertainties generated by the different geometries of the grates applied and any head variations over the inlet structure. Maximum discrepancies were observed immediately upstream and downstream of the inlet structure, likely due to the complex flow patterns generated by the grate types. While it is not currently feasible to use such methods directly within full scale flood simulations (due to the small mesh sizes required), the work demonstrates the academic capability of the modelling technique and validates the model for supplementary studies. It was also noted that minor discrepancies in the calculation of flow depth propagated to the estimation of flow exchange by the numerical model. Further, more detailed investigation of the exchange flows and the development of modelling approaches that can inherently account for spatially variable energy losses, flow depths and flow exchange rates within different inlet configurations will require characterisation of the velocity fields such that a full understanding of the flow can be elucidated.

## ACKNOWLEDGEMENTS

This research was funded by EPSRC through a grant with the reference EP/K040405/1. The experiments were conducted in the Water Laboratory of the Civil and Structural Engineering Department of the University of Sheffield. Dr Lee acknowledges the support from the APEC Climate Center.

## REFERENCES

Almedeij, A. O. & Houghtalen, R. J. 2003 *Urban Hydrology: Hydraulics and Storm Water Quality*. John Wiley & Son, Hoboken, NJ.

Bazin, P. H., Nakagawa, H., Kawaike, K., Paquier, A. & Mignot, E. 2014 Modeling flow exchanges between a street and an underground drainage pipe during urban floods. *Journal of Hydraulic Engineering* **140** (10), 04014051.

Chen, A., Djordjević, S., Leandro, J. & Savić, D. 2007 The urban inundation model with bidirectional flow interaction between 2D overland surface and 1D sewer networks.

In: *NOVATECH 2007 – Sixth International Conference on Sustainable Techniques and Strategies in Urban Water Management*, Lyon, France, pp. 465–472.

Djordjević, S., Prodanović, D., Maksimović, C., Ivetić, M. & Savić, D. 2005 SIPSON-simulation of interaction between pipe flow and surface overland flow in networks. *Water Science and Technology* **52** (5), 275–283.

Djordjević, S., Saul, A. J., Tabor, G. R., Blanksby, J., Galambos, I., Sabtu, N. & Sailor, G. 2013 Experimental and numerical investigation of interactions between above and below ground drainage systems. *Water Science and Technology* **67** (3), 535–542.

Gómez, M. & Russo, B. 2009 Hydraulic efficiency of continuous transverse grates for paved areas. *Journal of Irrigation and Drainage Engineering* **135** (2), 225–230.

Gómez, M. & Russo, B. 2011a Methodology to estimate hydraulic efficiency of drain inlets. *Proceedings of the Institution of Civil Engineers* **164** (2), 81–90.

Gómez, M., Macchione, F. & Russo, B. 2011b Methodologies to study the surface hydraulic behaviour of urban catchments during storm events. *Water Science and Technology* **63** (11), 2666–2673.

Gómez, M., Hidalgo, G. & Russo, B. 2013 Experimental campaign to determine grated inlet clogging factors in an urban catchment of Barcelona. *Urban Water Journal* **10** (1), 50–61.

Guo, J. C. 2000a Design of grate inlets with clogging factor. *Advances in Environmental Research* **4**, 181–186.

Guo, J. C. 2000b Street stormwater conveyance capacity. *Journal of Irrigation and Drainage Engineering* **72** (5), 626–630.

Haleem, D. A., Kesserwani, G. & Caviedes-Voullième, D. 2015 Haar wavelet-based adaptive finite volume shallow water solver. *Journal of Hydroinformatics* **17** (6), 857–873.

Hammond, M., Chen, A. S., Djordjevic, S., Butler, D. & Mark, O. 2015 Urban flood impact assessment: a state-of-the-art review. *Urban Water Journal* **12** (1), 14–29.

Larson, C. L. 1947 *Investigation of Flow Through Standard and Experimental Grate Inlets for Street Gutters*, Project Report, St Antony Falls Hydraulic Laboratory, University of Minesota.

Leandro, J., Chen, A., Djordjević, S. & Savić, D. 2009 Comparison of 1D/1D and 1D/2D coupled (sewer/surface) hydraulic models for urban flood simulation. *Journal of Hydraulic Engineering* **135**, 495–504. http://dx.doi.org/10.1061/(ASCE)HY.1943-7900.0000037#sthash.1QracRZb.dpuf.

Leandro, J., Lopes, P., Carvalho, R., Pascoa, P., Martins, R. & Romagnoli, M. 2014 Numerical and experimental characterization of the 2D vertical average-velocity plane at the centre-profile and qualitative air entrainment inside a gully for drainage and reverse flow. *Journal Computer & Fluids* **102**, 52–61.

Lee, S., Nakagawa, H., Kawaike, K. & Zhang, H. 2013 Experimental validation of interaction model at storm drain for development of integrated urban inundation model. *Journal of Japan Society of Civil Engineers, Ser. B1 (Hydraulic Engineering)* **69** (4), 109–114.

Lee, S. 2013 *Study on Development of Integrated Urban Inundation Model Incorporating Drainage Systems*. PhD Thesis, Kyoto University.

Li, W. H., Geyer, J. C. & Benton, G. S. 1951 Hydraulic behaviour of stormwater inlets: I. Flow into gutter inlets in straight gutter without depression. *Sewage and Industrial Wastes* **23** (1), 34–46.

Li, W. H., Goodel, B. C. & Geyer, J. C. 1954 Hydraulic behavior of stormwater inlets: IV. Flow into depressed combination inlets. *Sewage and Industrial Wastes* **26** (8), 967–975.

Lopes, P., Leandro, J., Carvalho, R. F., Páscoa, P. & Martins, R. 2015 Numerical and experimental investigation of a gully under surcharge conditions. *Urban Water Journal* **12**, 468–476.

Martins, R., Leandro, J. & Carvalho, R. F. 2014 Characterization of the hydraulic performance of a gully under drainage conditions. *Water Science and Technology* **69** (12), 2423–2430.

Martins, R., Kesserwani, J., Rubinato, M., Lee, S., Leandro, J., Djordjević, S. & Shucksmith, J. 2017a Validation of 2D shock capturing flood models around a surcharging manhole. *Urban Water Journal* **14** (9), 892–899. http://dx.doi.org/10.1080/1573062X.2017.1279193.

Martins, R., Leandro, J., Chen, A. & Djordjević, S. 2017b A comparison of three dual drainage models: shallow water vs local inertia vs diffusive wave. *Journal of Hydroinformatics* **19** (1). doi:10.2166/hydro.2017.075.

Rubinato, M. 2015 *Physical Scale Modelling of Urban Flood Systems*. PhD Thesis, University of Sheffield, http://etheses.whiterose.ac.uk/9270/.

Rubinato, M., Seungsoo, L., Kesserwani, G. & Shucksmith, J. 2016 Experimental and numerical investigation of water depths around a manhole under drainage conditions. In: *12th International Conference on Hydroinformatics-Smart Water for the Future*, 21–26 August, Songdo Convensia, Incheon, South Korea.

Rubinato, M., Martins, R., Kesserwani, J., Leandro, J., Djordjević, S. & Shucksmith, J. 2017a Experimental calibration and validation of sewer/surface flow exchange equations in steady and unsteady flow conditions. *Journal of Hydrology* **552**, 421–432. https://doi.org/10.1016/j.jhydrol.2017.06.024.

Rubinato, M., Martins, R., Kesserwani, G., Leandro, J., Djordjevic, S. & Shucksmith, J. 2017b Experimental investigation of the influence of manhole grates on drainage flows in urban flooding conditions. In: *14th IWA/IAHR International Conference on Urban Drainage*, 10–15 September, Prague, Czech Republic.

Ten Veldhuis, J. A. E. & Clemens, F. H. L. R. 2010 Flood risk modelling based on tangible and intangible urban flood damage quantification. *Water Science and Technology* **62** (1), 189–195.

Wang, Y., Liang, Q., Kesserwani, G. & Hall, J. W. 2011 A 2D shallow flow model for practical dam-break simulations. *Journal of Hydraulic Research* **49** (3), 307–316.

Xia, X., Liang, Q., Ming, X. & Hou, J. 2017 An efficient and stable hydrodynamic model with novel source term discretisation schemes for overland flow and flood simulations. *Water Resources Research* **53**. doi:10.1002/2016WR020055.

First received 5 October 2017; accepted in revised form 22 February 2018. Available online 9 April 2018